Energy Proceedings
Vol 57, 2025
ISSN 2004-2965

The miscible behaviors and mechanism of CO_2 and crude oil within nanoslits in ultra-deep reservoir: molecular dynamic simulation

Zechen Yan[1], Xiaofang Li[1*], Boxin Ding[2], Lei Zhu[1], Haonan Li[1], Chao Yan[1], Sen Wang[3], Qingzhong Xue[1], Bo Liao[3*]

1 Shandong Key Laboratory of Intelligent Energy Materials, School of Materials Science and Engineering, State Key Laboratory of Deep Oil and Gas, China University of Petroleum (East China), Qingdao 266580, Shandong, P. R. China

2 College of Petroleum Engineering, China University of Petroleum-Beijing, Beijing 102249, P. R. China

3 School of Petroleum Engineering, China University of Petroleum (East China), Qingdao 266580, Shandong, P. R. China
(*Xiaofang Li: lixiaofang@upc.edu.cn, Bo Liao: liaob@upc.edu.cn)

ABSTRACT

It is crucial to expose the miscible mechanism of CO_2 and crude oil for the development of ultra-deep reservoirs. The influence of oil composition and electrical properties of rock surface on the miscible process of CO_2 and crude oil (C_7H_{16}, $C_7H_{16}S$, $C_7H_{17}N$, $C_7H_{16}O$, $C_7H_{14}O_2$, C_9H_{20}, $C_{11}H_{24}$) at 453 K and 90 MPa is investigated by using the molecular dynamics simulation. The simulation results indicate that the adsorption of CO_2 and C_7H_{16} on the calcite surface limits the diffusion of CO_2 and C_7H_{16} along the Z direction. Meanwhile, high pressure could weaken the effect of temperature on the adsorption of CO_2 and C_7H_{16} on the calcite surface. In addition, the functional group and long chain of crude oil molecules adversely affect the miscibility between crude oil and CO_2. Moreover, the positively charged surface could promote the miscibility of C_7H_{16} and CO_2. The miscibility of $C_7H_{14}O_2$ and CO_2 could be facilitated in nanoslits with the same surface charges while it could be hindered in nanoslits with the opposite charges. This work could shed new light on the further research on the application of CO_2 flooding in ultra-deep reservoirs.

Keywords: Ultra-deep reservoir, CO_2 flooding, molecular dynamics simulation; miscible mechanism

1. INTRODUCTION

With the constant expanding of the oil demand and the depletion of conventional medium-shallow reservoirs, deep reservoirs (the drilling depth is from 4500 to 6000 meters) and ultra-deep reservoirs (the drilling depth exceeds 6000 meters) have become the main development target of oil exploration in the world due to the abundant oil reserves[1–5]. However, ultra-deep reservoirs are characterized by high temperature, high pressure, deep burial depth, strong heterogeneity and complex geological conditions, which are difficult to be extracted by conventional methods[6–9]. Although the hydraulic fracturing and horizontal drilling technologies significantly boost the commercial oil production in recent years, large amounts of crude oil tend to be still remaining in reservoirs owing to the tightness of the formation[10,11]. Thus, it is crucial to explore more feasible methods for effectively improving oil recovery in ultra-deep reservoirs.

Gas flooding has been identified as an efficient method to enhance oil recovery (EOR) through extensive experimental and numerical studies because of the easier injection approach and the higher efficiency of sweep[12,13]. Compared with N_2 and natural gases, CO_2 could be more easily miscible with crude oil under high temperature and high pressure, particularly for ultra-deep reservoirs with microscale and nanoscale pore structures, showing the considerable potential in EOR techniques[14–18]. Meanwhile, injecting CO_2 has attracted the higher attention against the global background of carbon emissions control, which could not only conquer energy resource extraction issues, but also provide the possibility to achieve CO_2 sequestration[19,20].

Compared with experimental methods limited by deep conditions, the molecular dynamics (MD) simulation could be a valuable tool for investigating the dynamics, thermodynamic and energetic properties of complex nanoscale systems from a molecular scale, which has become the bridge to connect the micro-scale phenomenon and macroscale properties[21,22]. Zhang et

This is a paper for International CCUS Conference 2025 (ICCUSC 2025), May 28-29, 2025, Beijing, China.

al.[23] reported the structural and dynamic properties of CO_2 and nC_8H_{18} mixtures in calcite nanopores. It was found that nC_8H_{18} molecules could be displaced by CO_2 on the pore surface at the low CO_2 content condition, while CO_2 adsorption on the pore surface was wholly saturated and CO_2 was able to mix with nC_8H_{18} in the bulk phase at the high CO_2 content condition, significantly decreasing the effective viscosity of CO_2-nC_8H_{18} mixtures. Li et al.[24] proved that high temperature and high pressure were favorable for oil-gas miscibility. In addition, the gas type had the remarkable influence on the displacement performance in both medium-shallow reservoirs and deep reservoirs with the sequence of $CO_2 > C_3H_8 > CH_4 > N_2$. Wang et al.[25] demonstrated that CO_2 flooding was more applicable for reservoirs with a high content of polar crude oil than hydrocarbon gas flooding and N_2 flooding. These findings could play a guiding role in the exploration of the miscible mechanism and behavior of CO_2 and crude oil in nanoslits.

Furthermore, the relevant studies have reported that the rock surface characteristics have a vital effect on the miscibility between crude oil and CO_2[26]. The fluid features in carbonate rocks have been widely researched in recent years[27–29]. Sun et al.[30] investigated the adsorption behaviors of CH_4 and CO_2 in slit nanopores with various surface compositions. Due to the stronger adsorption interactions between the CO_2 molecules and the calcite surface, CH_4 could be widely replaced by CO_2 on the calcite surface. Notably, previous studies primarily focused on neutral carbonate surface rocks[31] while most carbonate surfaces are electrical[32]. It has been proved that the polarizability of calcite mineral surfaces could affect dramatically the interactions between crude oil and rock surfaces[33–35]. However, there are few pieces of research on charged surfaces. Therefore, it is meaningful to study the miscible characteristics of crude oil and CO_2 in charged carbonate reservoirs.

In summary, although there have been extensive investigations on the application of CO_2 flooding in reservoir development, the research on the miscible process and mechanism of CO_2 and crude oil in ultra-deep reservoirs, especially for polar crude oil components and charged calcite surfaces, is still deficient. To solve the above problems, the miscible behavior and mechanism of CO_2 and crude oil in ultra-deep reservoirs are systematically studied by the MD simulation method. The selected temperatures are 413 K, 433 K, 453 K, 473 K and 493 K, and the selected pressures are 50 MPa, 70 MPa and 90 MPa, respectively. The present study is basically divided into the following three parts: (1) the diffusion and adsorption processes of CO_2 and C_7H_{16} system are studied at different temperature and pressure, (2) the effect of crude oil type on the miscible process of oil molecules and CO_2 is investigated, including functional group and chain length, (3) the influence of calcite surface properties on the miscible process of CO_2 and apolar/polar crude oil is discussed.

2. MODELS AND METHODS

In this study, Materials Studio (MS) computer simulation software package was adopted to perform all MD simulations. The Condensed-phase Optimized Molecular Potentials for Atomistic Simulation Studies (COMPASS) force field[36] was used to depict interactions and miscible properties of CO_2 phase and oil phase[37]. All systems were geometrically optimized before dynamic simulations. Bonding energy and non-bonding energy played a significant role in the COMPASS force field, where the non-bonding energy included van der Waals (vdW) interactions and electrostatic interactions. The vdW interactions were calculated by the 9-6 Lennard-Jones potential function with a cut-off distance of 15.5 Å and the electrostatic interactions were computed by the Coulomb potential[25]. All MD simulations were carried out under the NPT (constant number of atoms, constant pressure, constant temperature) ensemble and the NVT (constant number of atoms, constant volume, constant temperature) ensemble. The temperature and pressure of the systems were controlled by Andersen thermostat and Berendsen methods, respectively. The data was collected every 5 ps with a fixed time step of 1 fs. The simulation time was sufficient for all MD systems because the variation of the total energy of all MD systems was slight with the increasing simulation time.

Additionally, density functional theory simulations were chosen to calculate the dipole moments of different oil molecules. Generalized gradient approximation with the Perdew-Burke-Ernzerhof was employed for exchange and correlation potential function. A double numerical basis set with polarization function was applied. To acquire high-quality simulation results, the convergence tolerances were 1×10^{-6} Ha (1 Ha = 27.2114 eV) for the total energy, 0.02 Ha/nm for atomic forces, 5×10^{-4} nm for maximum displacement, respectively.

The MD system consisted of CO_2 phase, oil phase, calcite surface and helium (He) nanosheet. Herein, He

nanosheets were fixed to keep the constant volume of oil phase and CO_2 phase. Fig. 1 showed (a) CO_2, (b) C_7H_{16}, (c) $C_7H_{16}S$, (d) $C_7H_{17}N$, (e) $C_7H_{16}O$, (f) $C_7H_{14}O_2$, (g) C_9H_{20}, (h) $C_{11}H_{24}$, (i) the neutral surface and (j) the charged surface. The neutral surface and charged surface were produced by cleaving calcite along the (104) and the (001) crystallographic orientation and its dimensions (X Y Z) were 14.0 × 3.0 × 1.5 nm^3, respectively. The Neutral System (NS) was composed of two parallel neutral surfaces with a pore width of 7 nm, as presented in Fig. 2. The part of calcite surfaces was fixed. CO_2 and crude oil molecules were placed on both sides of the nanoslits. For each system, the number of CO_2 and crude oil molecules was determined according to the density of CO_2 and crude oil.

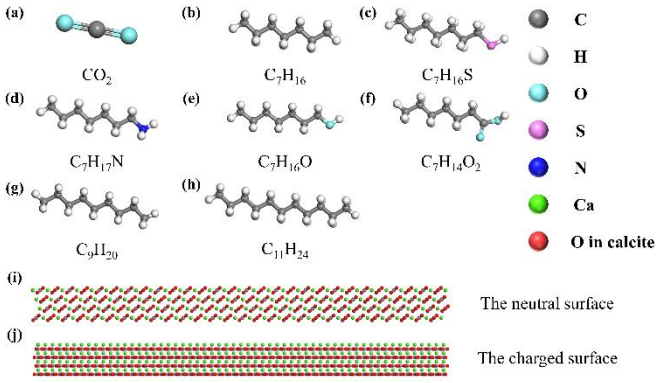

Fig. 1. (a) CO_2, (b-h) crude oil and (i-j) calcite models used in this study

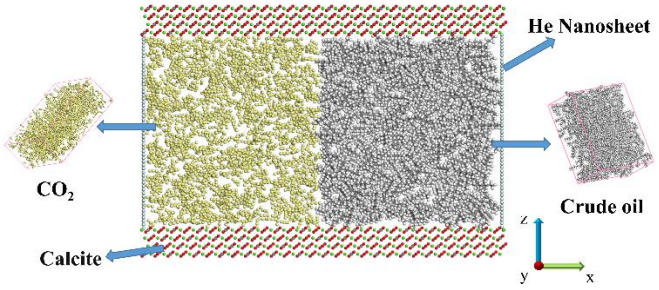

Fig. 2. The initial miscible system used in the simulation

3. RESULTS AND DISCUSSIONS

3.1 Temperature and pressure

Herein, the diffusion and adsorption process of CO_2 and C_7H_{16} in calcite nanoslits is studied at 453 K and 90 MPa. The diffusion coefficients (D) are employed to depict the diffusion characteristics of CO_2 and C_7H_{16} along the X and Z directions, as depicted in Fig. 3. The detailed D of CO_2 and C_7H_{16} are computed by equation (1), respectively,

$$D=\lim_{t\to\infty}\frac{\left\langle |r(t)-r(0)|^2\right\rangle}{6t} \quad (1)$$

where <...> is the averaging over all the molecules, D is the diffusion coefficient (m^2/s), $r(t)$-$r(0)$ represents the displacement of the center mass of a molecule, t represents simulation time. The figure illustrates that the diffusion velocity of CO_2 is much higher than that of C_7H_{16} at the initial simulation time. However, the diffusion velocity of CO_2 shows a sharp decrease while the diffusion velocity of C_7H_{16} manifests a slight decrease along X and Z directions with increasing simulation time. In addition, the diffusion coefficient along the X direction is larger than that along the Z direction because of the adsorption of CO_2 and C_7H_{16} on the calcite surface. The diffusion coefficient along the Z direction is close to zero at the later stage of the simulation, meaning that the adsorption of CO_2 and C_7H_{16} on the calcite surface reaches the equilibrium state.

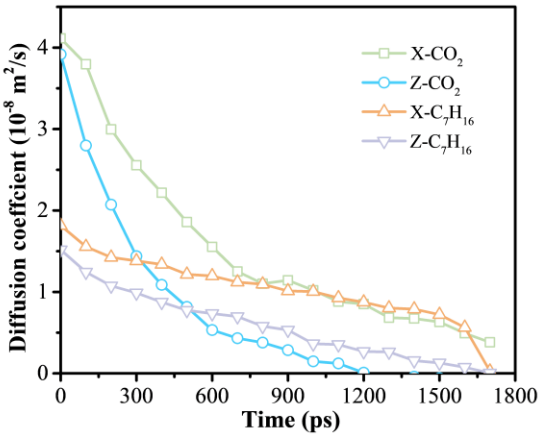

Fig. 3. At 453 K and 90 MPa, the variation of the diffusion coefficients of CO_2 and C_7H_{16} versus the simulation time

To certify the above conclusions, the interaction energies between CO_2/C_7H_{16} and rock surface are computed according to equation (2) and equation (3),

$$E_{Sur\,/\,CO_2}=\frac{E_{Sur+CO_2}-(E_{Sur}+E_{CO_2})}{N_{CO_2}} \quad (2)$$

$$E_{Sur\,/\,C_7H_{16}}=\frac{E_{Sur+C_7H_{16}}-(E_{Sur}+E_{C_7H_{16}})}{N_{C_7H_{16}}} \quad (3)$$

where $E_{sur/CO2}$ is the interaction energy between CO_2 phase and calcite surface, $E_{sur+CO2}$ is the total energy of CO_2 phase and calcite surface, $E_{sur/C7H16}$ is the interaction energy between C_7H_{16} phase and calcite surface, $E_{sur+C7H16}$ is the total energy of C_7H_{16} phase and calcite surface, E_{sur}, E_{CO2} and E_{C7H16} represent the energy of calcite surface,

CO_2 phase and C_7H_{16} phase, respectively, N_{CO2} and N_{C7H16} represent the number of CO_2 molecules and C_7H_{16} molecules, respectively. It is discovered in Fig. 4a and Fig. 4c that $E_{sur/CO2}$ and $E_{sur/C7H16}$ increase as increasing simulation time at the early stage of simulation, which are gradually stable with increasing simulation time. Additionally, the relative concentrations of CO_2 and crude oil indicate that CO_2 has a monolayer adsorption and C_7H_{16} has a double-layer adsorption as simulation time increases, as depicted in Fig. 4b and Fig. 4d.

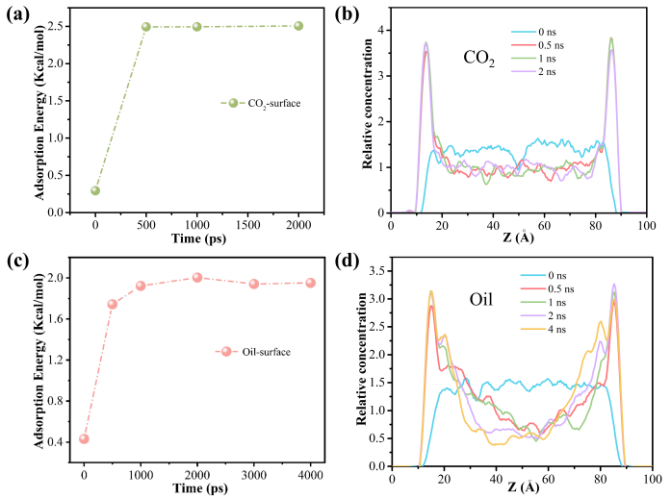

Fig. 4. At 453 K and 90 MPa, the adsorption energy of (a) CO_2 and (c) C_7H_{16} with the rock surface, the relative concentration of (b) CO_2 and (d) C_7H_{16} along the Z direction

Furthermore, the diffusion and adsorption processes of CO_2 and C_7H_{16} in calcite nanoslits at different temperatures and pressures are studied in this section, where $E_{sur/CO2}$ and $E_{sur/C7H16}$ are calculated in Fig. 5. Clearly, under different temperature conditions, the difference of $E_{sur/CO2}$ at the lower pressure is significantly larger than that at the higher pressure. For instance, at 50 MPa, the value of $E_{sur/CO2}$ at 493 K (1.938 Kcal/mol) is 21.05% higher than that at 413 K (1.601 Kcal/mol) while the value of $E_{sur/CO2}$ at 493 K (1.427 Kcal/mol) is close to that at 413 K (1.418 Kcal/mol) at 90 MPa. Compared with the difference of $E_{sur/CO2}$, under the different temperatures, the difference of $E_{sur/C7H16}$ at low pressure is slightly larger than that at high pressure. At 50 MPa, the value of $E_{sur/C7H16}$ at 413 K (0.930 Kcal/mol) is 3.9% higher than that at 493 K (0.895 Kcal/mol). At 90 MPa, the value of $E_{sur/C7H16}$ at 413 K (0.89593 Kcal/mol) approaches that at 493 K (0.89597 Kcal/mol). Accordingly, it could draw a conclusion that temperature shows the slight effect on the adsorption of CO_2 and C_7H_{16} on the calcite surface at high pressure.

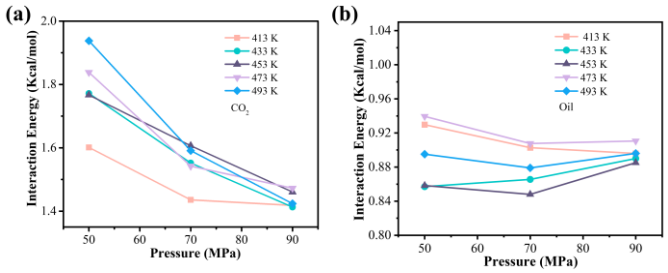

Fig. 5. (a) $E_{sur/CO2}$ and (b) $E_{sur/C7H16}$ at different temperatures and pressures

3.2 *Crude oil composition*

Crude oil composition could affect the miscible properties of CO_2 and crude oil in calcite nanoslits[25]. Accordingly, the effect of functional group and chain length of crude oil on the miscible processes between crude oil and CO_2 is investigated and the underlying mechanism is uncovered.

3.2.1 Functional group

Herein, $C_7H_{16}S$, $C_7H_{17}N$, $C_7H_{16}O$ and $C_7H_{14}O_2$, containing mercaptan, amino, hydroxyl and carboxyl groups, respectively, are selected to compare with C_7H_{16}. Fig. 6 presents the miscible processes of CO_2 and different crude oil at 453 K and 90 MPa. It could be found that CO_2 molecules and oil molecules are placed in the calcite nanoslits with a well-defined interface at the initial state for the five systems. As the simulation time increases, the interfaces between C_7H_{16}/$C_7H_{16}S$ phase and CO_2 phase are gradually blurred and C_7H_{16}/$C_7H_{16}S$ molecules diffuse into the CO_2 phase, showing the better miscibility between C_7H_{16}/$C_7H_{16}S$ and CO_2. In contrast, the proportion of $C_7H_{17}N$, $C_7H_{16}O$ and $C_7H_{14}O_2$ molecules in CO_2 phase is less than that of C_7H_{16} and $C_7H_{16}S$ molecules. Because more $C_7H_{17}N$, $C_7H_{16}O$ and $C_7H_{14}O_2$ molecules are absorbed on the calcite surface or remain in the initial position, leading to a lower miscibility with CO_2. Fig. 7a exhibits the relative concentration distribution of crude oil along the Z direction. It could be seen that there exist two adsorption peaks of $C_7H_{17}N$, $C_7H_{16}O$ and $C_7H_{14}O_2$ in the ranges of 11 Å-14 Å and 86 Å-89 Å, respectively. However, the concentration distribution of C_7H_{16} and $C_7H_{16}S$ is approximately zero in these ranges. These phenomena demonstrate that CO_2

could replace C_7H_{16} and $C_7H_{16}S$ on the calcite surface, which could not replace $C_7H_{17}N$, $C_7H_{16}O$ and $C_7H_{14}O_2$.

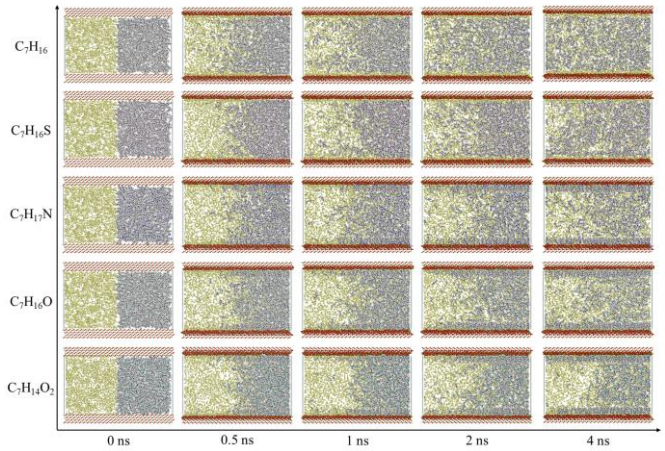

Fig. 6. The miscible process of CO2 and crude oil at 453 K and 90 MPa

To elucidate the impact of functional group on the miscible process of crude oil and CO_2, the miscibility (M) between oil molecules and CO_2 at 453 K and 90 MPa is calculated[38]. The calculation equation is as follows,

$$M = \frac{N_2}{N_1} \quad (4)$$

where N_1 represents the number of oil molecules in free state, N_2 represents the number of oil molecules dissolved in CO_2 phase. Fig. 7b illustrates the miscibility values of different oil molecules in CO_2 phase at 4 ns. It is obvious that the order of M values is C_7H_{16} (0.42) > $C_7H_{16}S$ (0.38) > $C_7H_{17}N$ (0.29) > $C_7H_{16}O$ (0.27) > $C_7H_{14}O_2$ (0.10). The above results show that the miscibility of CO_2 and C_7H_{16} is higher than that of CO_2 and other crude oil, indicating that functional groups could have a negative effect on the miscible process of CO_2 and crude oil. In addition, there are differences in the effects of various functional groups on the miscibility of crude oil and CO_2. For instance, the M value of $C_7H_{16}S$ (0.38) is close to the M value of C_7H_{16} (0.42) while is 41% larger than that of $C_7H_{16}O$ (0.27). To investigate the reason of the above phenomenon, the dipole moment of crude oil is calculated, as shown in Table 1. The dipole moment is often used to quantificationally depict the polarity of oil molecules[39]. It could be discovered that the dipole moments of C_7H_{16}, $C_7H_{16}S$ and $C_7H_{16}O$ are 0.0955 Debye, 1.5913 Debye and 1.5988 Debye, respectively, indicating that C_7H_{16} is an apolar molecule and $C_7H_{16}S$ and $C_7H_{16}O$ belong to polar molecules. Based on the above results, it is proved that polarity could not be the major factor for the miscibility of crude oil and CO_2.

Table 1. The dipole moments (Debye) of different crude oil molecules

Oil type	C_7H_{16}	$C_7H_{16}S$	$C_7H_{17}N$	$C_7H_{16}O$	$C_7H_{14}O_2$
Dipole moment	0.0955	1.5913	1.2205	1.5988	3.98

To reveal the mechanism of functional groups affecting miscibility, the interaction energy between rock surface and crude oil molecules is computed in Fig. 8. It could be observed that the interaction energy between rock surface and oil ($C_7H_{17}N$, $C_7H_{16}O$ and $C_7H_{14}O_2$) is significantly stronger than that for rock surface and C_7H_{16}/$C_7H_{16}S$, which is the main reason for the adsorption of $C_7H_{17}N$, $C_7H_{16}O$ and $C_7H_{14}O_2$ molecules on the rock surface. Furthermore, electrostatic energy is the main driving force for $C_7H_{17}N$, $C_7H_{16}O$ and $C_7H_{14}O_2$, while vdW interaction is the main driving force for $C_7H_{16}S$ and C_7H_{16}. The relevant studies have shown that S atoms have stronger Lennard-Jones interactions than C, N and O atoms, while Lennard-Jones interactions could be disrupted by high temperature, which could reduce the vdW interactions[40]. The above discussions could well explain the miscible behavior and molecular distribution

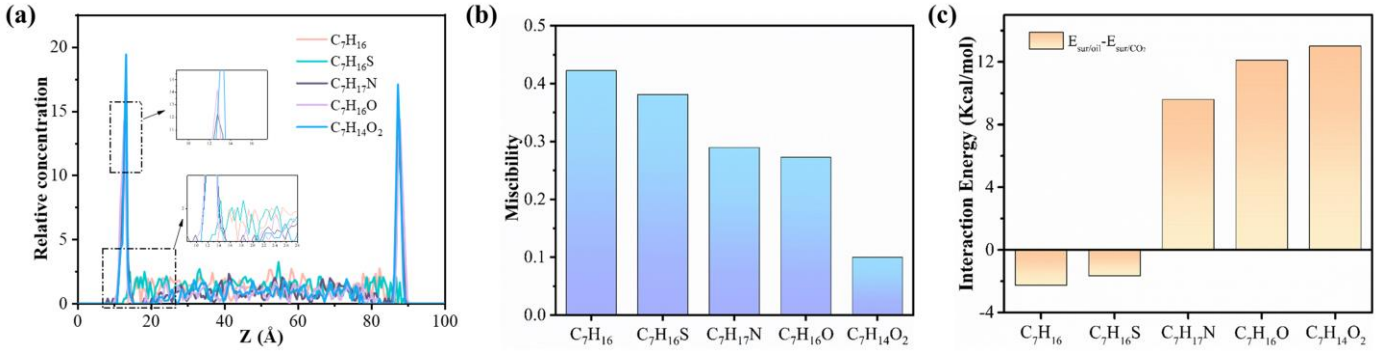

Fig. 7. (a) The relative concentration along the Z direction of different crude oils; (b) The miscibility between different crude oils and CO_2; (c) The difference between $E_{sur/oil}$ and $E_{sur/CO2}$

of $C_7H_{16}S$ at 453 K and 90 MPa. Thus, it could be concluded that the interaction energy might be the key factor for the miscibility of crude oil and CO_2 in the ultra-deep reservoir.

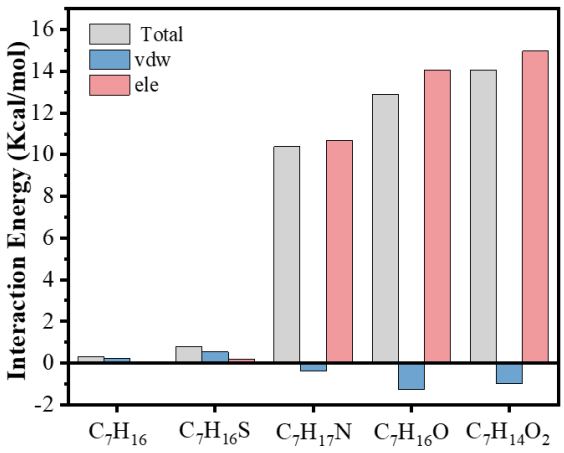

Fig. 8. The interaction energy between rock surface and crude oil at 453 K and 90 MPa

In order to verify the above conclusion, the difference between $E_{sur/oil}$ and $E_{sur/CO2}$ to describe the interaction between CO_2 and crude oil is analyzed. Fig. 7c shows that the sequence of $E_{sur/oil}$-$E_{sur/CO2}$ at 4 ns is C_7H_{16} < $C_7H_{16}S$ < $C_7H_{17}N$ < $C_7H_{16}O$ < $C_7H_{14}O_2$. The M values of different oil molecules follow the order of C_7H_{16} > $C_7H_{16}S$ > $C_7H_{17}N$ > $C_7H_{16}O$ > $C_7H_{14}O_2$. Consequently, the smaller value of $E_{sur/oil}$-$E_{sur/CO2}$, the better miscibility between crude oil and CO_2. The aforementioned results certify that the miscibility between crude oil and CO_2 is not mainly determined by polarity and is mainly related to the competitive adsorption between oil and CO_2 on the rock surface.

3.2.2 Chain length of crude oil

The miscible processes between C_7H_{16}/C_9H_{20}/$C_{11}H_{24}$ and CO_2 are studied in this section. Here, the calculated M values manifest that C_7H_{16} and CO_2 show better miscibility compared with C_9H_{20} and $C_{11}H_{24}$ (Fig. 9b). In order to demonstrate abovementioned results, the interaction energy between CO_2 and crude oil is calculated according to equation (4), as illustrated in Fig. 9a,

$$E_{oil\ /\ CO_2} = \frac{E_{oil\ +\ CO_2} - (E_{oil} + E_{CO_2})}{N_{oil}} \quad (4)$$

where $E_{oil/CO2}$ is the interaction energy between CO_2 phase and crude oil, $E_{oil+CO2}$ is the total energy of CO_2 phase and crude oil, E_{CO2} and E_{oil} represent the energy of CO_2 phase and oil phase, respectively, N_{oil} represents the number of crude oil molecules. It could be seen that the interaction energy between CO_2 and crude oil follows the order of C_7H_{16} < C_9H_{20} < $C_{11}H_{24}$, indicating that the interaction energy between CO_2 and crude oil increases with increasing chain length of crude oil. Accordingly, it indicates that the interaction energy between CO_2 and crude oil is not the major factor affecting the miscibility. To further clarify the mechanism of chain length affecting miscibility between CO_2 and crude oil, the diffusion coefficients of crude oil is calculated in Fig. 9b. It shows the order of the diffusion velocity of C_7H_{16} > C_9H_{20} > $C_{11}H_{24}$, which is consistent with that of the miscibility between CO_2 and crude oil. Furthermore, the literature has demonstrated that the longer chain crude oil has a higher molecular weight and larger molecular interaction, resulting in a weaker diffusion coefficient[41]. Based on the above analysis, it could be concluded that CO_2 shows better miscibility with short-chain crude oil owing to the larger diffusion velocity.

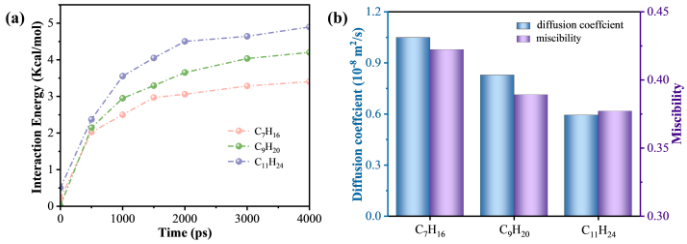

Fig. 9. (a) The interaction energy between different crude oils and CO_2; (b) The calculated diffusion coefficients of different crude oils and the miscibility between crude oil and CO_2

3.3 The electrical property of the rock surface

To explore the effect of the electrical properties of rock surfaces on the miscible process, Charged System (CS), Positively Charged System (CS-P) and Negatively Charged System (CS-N) are constructed for comparison with the NS system. The CS system is the nanoslits with positive charges on the lower surface and negative charges on the upper surface[32]. The CS-P system is the nanoslits comprised of positively charged surfaces and the CS-N system is the nanoslits comprised of negatively charged surfaces.

3.3.1 Apolar molecules

Fig. 10a exhibits the miscibility between C_7H_{16} and CO_2 in four systems. It could be observed that C_7H_{16} exhibits greater miscibility in the CS and CS-P systems than that in the NS and CS-N systems. Both CS and CS-P systems contain positively charged surfaces. Accordingly, it is assumed that the positively charged surface could promote the miscibility of C_7H_{16} and CO_2. To confirm this assumption, the relative concentration distribution of CO_2 along the Z direction is plotted. Fig. 10b and 10c depict that the relative distribution of CO_2 in four systems is different and the thickness of the CO_2 adsorption layer follows the order of positively charged surface < neutral surface < negatively charged surface. This phenomenon could be attributed to the orientation of CO_2 adsorbed on the rock surface (Fig. 11). The negatively charged O atom of CO_2 is attracted by Ca^{2+} on the positively charged surface, causing some CO_2 molecules to be largely parallel to the rock surface. The positively charged C atom of CO_2 is drawn to CO_3^{2-} on the negatively charged surface and CO_2 tends to form a certain angle with the rock surface. In contrast, CO_2 orientation is unevenly and randomly distributed on the neutral surface. For a given pore size, CS and CS-P systems have larger miscibility of crude oil and CO_2 due to the thinner CO_2 adsorption layer on the positively charged surfaces compared with NS and CS-N systems. Because a thicker adsorption layer could result in a smaller pore size, which is disadvantageous for the oil-gas miscibility[42]. Based on the above discussions, it could be concluded that the miscibility between C_7H_{16} and CO_2 is higher in the nanoslits containing positively charged surfaces.

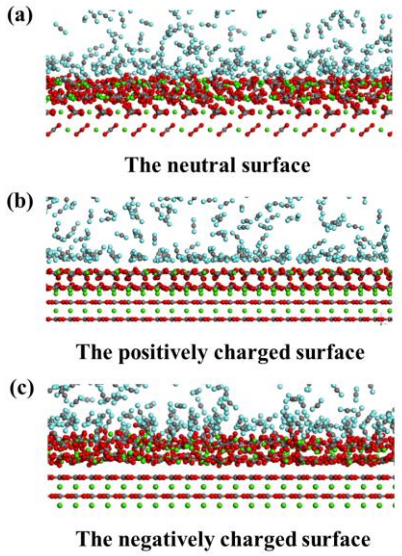

Fig. 11. The adsorption of CO_2 on each rock surface

3.3.2 Apolar molecules

Some MD simulations are performed to further study the effect of different electrical property systems on miscible processes of $C_7H_{14}O_2$ and CO_2 (Fig. 12a). In the NS, CS-P and CS-N systems, some $C_7H_{14}O_2$ molecules diffuse into CO_2 phase. However, in the CS system, $C_7H_{14}O_2$ molecules are difficult to diffuse, and most of the $C_7H_{14}O_2$ molecules are confined to the initial position. The miscibility between $C_7H_{14}O_2$ and CO_2 in the NS, CS-P and CS-N systems is obviously higher than that in the CS system (Fig. 12b), especially for CS-P and CS-N systems. For example, the M (0.192) in the CS-N systems is about twice as large as that (0.095) in the CS system. To explore the miscible mechanism, the adsorption energy of $C_7H_{14}O_2$ on the rock surface is calculated. Meanwhile, the figure exhibits that the adsorption energy of $C_7H_{14}O_2$ on the rock surface in the CS system is significantly higher than that in other three systems. To explain this

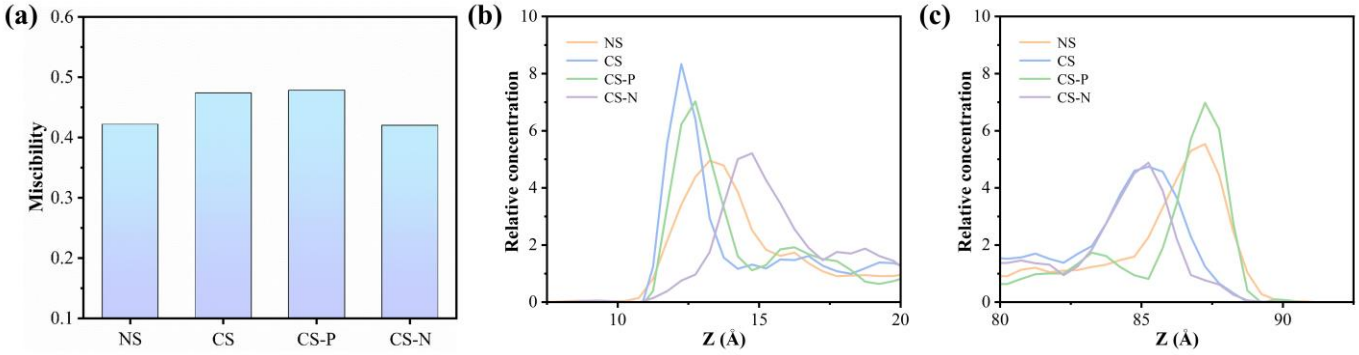

Fig. 10. (a) The miscibility between C_7H_{16} and CO_2 in four systems; (b) The relative concentration of CO_2 on the lower surface of the nanoslits along the Z direction; (c) The relative concentration of CO_2 on the upper surface of the nanoslits along the Z direction.

phenomenon, the relative concentration distribution of the two oxygen atoms of $C_7H_{14}O_2$ along the Z direction in the NS system and CS system is depicted in Fig. 12c. In the NS system, the relative concentration distribution profiles of the two types of oxygen atoms in $C_7H_{14}O_2$ basically coincide. However, in the CS system, there is a disparity of 2 Å in the distribution of O1 and O2 of $C_7H_{14}O_2$, which confirms that $C_7H_{14}O_2$ is ordered and has a certain molecular orientation in the CS system. It could be caused by the local electric field induced by the opposite charges on both sides of the rock, which is consistent with literature results[43]. According to the abovementioned discussions, a conclusion could be drawn that the miscibility between $C_7H_{14}O_2$ and CO_2 is hindered in the nanoslits with oppositely charged surfaces but is promoted in the nanoslits composed of the same charged surfaces.

affected by the competitive adsorption between CO_2 and crude oil instead of the polarity of crude oil molecules. The smaller value of $E_{sur/C7H16}$-$E_{sur/CO2}$, the better miscibility between crude oil and CO_2. Generally, functional groups adversely influence the miscible process between CO_2 and crude oil because of the strong interaction energy between crude oil and rock surface. $C_7H_{16}S$ shows a difference because high temperature could disrupt the interaction between $C_7H_{16}S$ and rock surface. Additionally, the increasing chain length of crude oil could hinder the miscibility between crude oil and CO_2. Thus, CO_2 flooding could be suitable for the high content of crude oil components with low carbon content and without functional groups.

Finally, the influence of electrical properties of rock surface on the miscibility between CO_2 and crude oil is explored. The miscibility between C_7H_{16} and CO_2 is higher

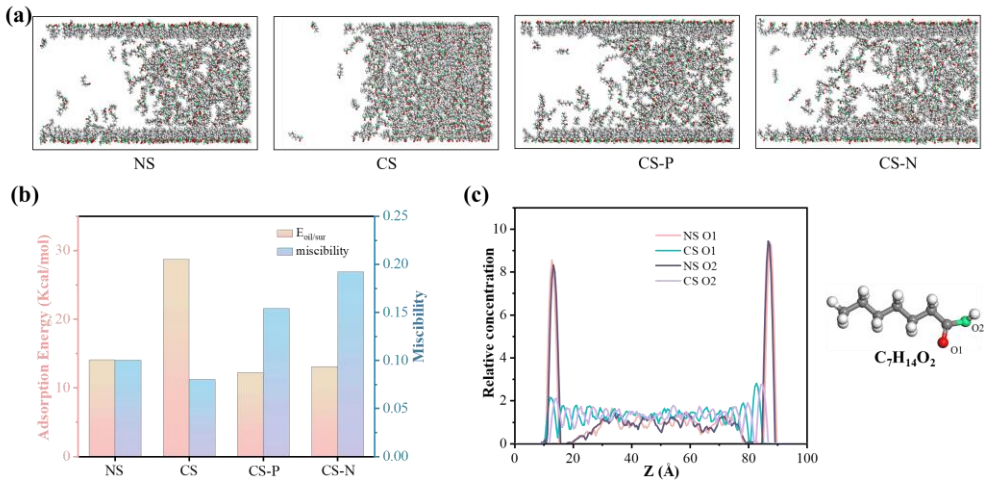

Fig. 12. (a) The adsorption configurations of $C_7H_{14}O_2$; (b) The adsorption energy of $C_7H_{14}O_2$ on the rock surface and the miscibility between $C_7H_{14}O_2$ and CO_2; (c) The relative concentration distribution of the two oxygen atoms of $C_7H_{14}O_2$ along the Z direction in NS and CS systems

4. CONCLUSIONS

In this work, the miscible behavior and mechanism of CO_2 and crude oil in calcite nanoslits under ultra-deep conditions are studied via MD simulations. The results indicate that the diffusion velocity of CO_2 shows a great decrease while the diffusion velocity of C_7H_{16} manifests a slight decrease along X and Z directions with increasing simulation time, which are caused by the variation of $E_{sur/CO2}$ and $E_{sur/C7H16}$. In addition, the influence of temperature on the adsorption of CO_2 and C_7H_{16} on the calcite surface could be negligible at high pressures.

Then, the effect of functional group and chain length of crude oil on the miscibility of crude oil and CO_2 is investigated under high temperature and high pressure. The miscibility of crude oil and CO_2 is mainly in the nanoslits containing positively charged surfaces, which is related to the thickness of the CO_2 adsorption layer. The miscibility between $C_7H_{14}O_2$ and CO_2 in the nanoslits composed of the same charges is higher than that in the nanoslits consisting of neutral surfaces and is lower in the nanoslits with oppositely charged surfaces due to forming a local electric field induced by the opposite charges. The above conclusions could be conducive to further research on the miscibility between CO_2 and crude oil in ultra-deep reservoirs.

ACKNOWLEDGEMENT

This work is supported by the Fundamental Research Funds for the Central Universities (24CX02007A, 24CX06005A), the Fund of State Key Laboratory of Deep

Oil and Gas, China University of Petroleum (East China), Shandong Key Laboratory of Intelligent Energy Materials, School of Materials Science and Engineering, China University of Petroleum (East China).

DECLARATION OF INTEREST STATEMENT

The authors declare that they have no known competing financial interests or personal relationships that could have appeared to influence the work reported in this paper. All authors read and approved the final manuscript.

REFERENCE

[1] Shen Y, Lü X, Guo S, Song X, Zhao J. Effective evaluation of gas migration in deep and ultra-deep tight sandstone reservoirs of Keshen structural belt, Kuqa depression. Journal of Natural Gas Science and Engineering 2017; 46: 119–31.

[2] Sheng JJ. Critical review of field EOR projects in shale and tight reservoirs. Journal of Petroleum Science and Engineering 2017; 159: 654–65.

[3] Yan Z, Li X, Zhu X, Wang P, Yu S, Li H, et al. MD-CFD simulation on the miscible displacement process of hydrocarbon gas flooding under deep reservoir conditions. Energy 2023; 263: 125730.

[4] Zhang Y, Gao M, You Q, Fan H, Li W, Liu Y, et al. Smart mobility control agent for enhanced oil recovery during CO_2 flooding in ultra-low permeability reservoirs. Fuel 2019; 241: 442–50.

[5] Saleh TA. Characterization, determination and elimination technologies for sulfur from petroleum: Toward cleaner fuel and a safe environment. Trends in Environmental Analytical Chemistry 2020; 25: e00080.

[6] Zhu G, Milkov AV, Chen F, Weng N, Zhang Z, Yang H, et al. Non-cracked oil in ultra-deep high-temperature reservoirs in the Tarim basin, China. Marine and Petroleum Geology 2018; 89: 252–62.

[7] Xu C, Zou W, Yang Y, Duan Y, Shen Y, Luo B, et al. Status and prospects of deep oil and gas resources exploration and development onshore China. Journal of Natural Gas Geoscience 2018; 3: 11–24.

[8] Waples DW. The kinetics of in-reservoir oil destruction and gas formation: constraints from experimental and empirical data, and from thermodynamics. Organic Geochemistry 2000; 31: 553–75.

[9] Yan Z, Zhu X, Wang P, Li X, Yu S, Li Y, et al. The effect of gas injection velocity and pore morphology on displacement mechanisms in porous media based on CFD approach. Journal of Natural Gas Science and Engineering 2022; 101: 104558.

[10] Vidic RD, Brantley SL, Vandenbossche JM, Yoxtheimer D, Abad JD. Impact of Shale Gas Development on Regional Water Quality. Science 2013; 340: 1235009.

[11] Kalam S, Afagwu C, Al Jaberi J, Siddig OM, Tariq Z, Mahmoud M, et al. A review on non-aqueous fracturing techniques in unconventional reservoirs. Journal of Natural Gas Science and Engineering 2021; 95: 104223.

[12] Wang Z-H, Sun B-W, Guo P, Wang S-S, Liu H, Liu Y, et al. Investigation of flue gas water-alternating gas (flue gas–WAG) injection for enhanced oil recovery and multicomponent flue gas storage in the post-waterflooding reservoir. Pet Sci 2021; 18: 870–82.

[13] Xue C, Ji D, Wen Y, Luo H, Zhao Y, Li Y. Promising combination of CO_2 enhanced oil recovery and CO2 sequestration in calcite nanoslits: Insights from molecular dynamics simulations. Journal of Molecular Liquids 2023; 391: 123243.

[14] Tang Y, Hou C, He Y, Wang Y, Chen Y, Rui Z. Review on Pore Structure Characterization and Microscopic Flow Mechanism of CO_2 Flooding in Porous Media. Energy Technology 2021; 9: 2000787.

[15] Zhang J, Pan Z, Liu K, Burke N. Molecular Simulation of CO_2 Solubility and Its Effect on Octane Swelling. Energy Fuels 2013; 27: 2741–7.

[16] Diffusion Coefficients in CO_2/n-Alkane Binary Liquid Mixtures by Molecular Simulation | The Journal of Physical Chemistry B n.d.

[17] Li C, Pu H, Zhao JX. Molecular Simulation Study on the Volume Swelling and the Viscosity Reduction of n-Alkane/CO_2 Systems. Ind Eng Chem Res 2019; 58: 8871–7.

[18] Li X, Wang S, Feng Q, Xue Q. The miscible behaviors of $C_{10}H_{22}$($C_7H_{17}N$)/C_3H_8 system: Insights from molecular dynamics simulations. Fuel 2020; 279: 118445.

[19] Wang X, van 't Veld K, Marcy P, Huzurbazar S, Alvarado V. Economic co-optimization of oil recovery and CO_2 sequestration. Applied Energy 2018; 222: 132–47.

[20] Middleton RS, Ogland-Hand JD, Chen B, Bielicki JM, Ellett KM, Harp DR, et al. Identifying geologic characteristics and operational decisions to meet global carbon sequestration goals. Energy Environ Sci 2020; 13: 5000–16.

[21] Yao H, Liu J, Xu M, Ji J, Dai Q, You Z. Discussion on molecular dynamics (MD) simulations of the asphalt materials. Advances in Colloid and Interface Science 2022; 299: 102565.

[22] Ma Z, Ranjith PG. Review of application of molecular dynamics simulations in geological sequestration of carbon dioxide. Fuel 2019; 255: 115644.
[23] Zhang W, Feng Q, Wang S, Xing X, Jin Z. CO_2-regulated octane flow in calcite nanopores from molecular perspectives. Fuel 2021; 286: 119299.
[24] Li S, Hao X, Yu S, Yan Y, Zhang J, Wang X. Influence of injected gas type and reservoir conditions on the oil migration in calcite nanoslits. Journal of Petroleum Science and Engineering 2022; 208: 109754.
[25] Wang P, Li X, Tao Z, Wang S, Fan J, Feng Q, et al. The miscible behaviors and mechanism of CO_2/CH_4/C_3H_8/N_2 and crude oil in nanoslits: A molecular dynamics simulation study. Fuel 2021; 304: 121461.
[26] Fang T, Zhang Y, Ding B, Yan Y, Zhang J. Static and dynamic behavior of CO_2 enhanced oil recovery in nanoslits: Effects of mineral type and oil components. International Journal of Heat and Mass Transfer 2020; 153: 119583.
[27] Kerisit S, Parker SC, Harding JH. Atomistic Simulation of the Dissociative Adsorption of Water on Calcite Surfaces. J Phys Chem B 2003; 107: 7676–82.
[28] Cooke DJ, Gray RJ, Sand KK, Stipp SLS, Elliott JA. Interaction of Ethanol and Water with the {10$\bar{1}$4} Surface of Calcite. Langmuir 2010; 26: 14520–9.
[29] Koleini MM, Badizad MH, Kargozarfard Z, Ayatollahi S. Interactions between Rock/Brine and Oil/Brine Interfaces within Thin Brine Film Wetting Carbonates: A Molecular Dynamics Simulation Study. Energy Fuels 2019; 33: 7983–92.
[30] Sun H, Zhao H, Qi N, Li Y. Effects of Surface Composition on the Microbehaviors of CH_4 and CO_2 in Slit-Nanopores: A Simulation Exploration. ACS Omega 2017; 2: 7600–8.
[31] Bai S, Kubelka J, Piri M. A positively charged calcite surface model for molecular dynamics studies of wettability alteration. Journal of Colloid and Interface Science 2020; 569: 128–39.
[32] Zhao J, Yao G, Ramisetti SB, Hammond RB, Wen D. Molecular dynamics investigation of substrate wettability alteration and oil transport in a calcite nanopore. Fuel 2019; 239: 1149–61.
[33] Kanj M, Sakthivel S, Giannelis E. Wettability Alteration in Carbonate Reservoirs by Carbon Nanofluids. Colloids and Surfaces A: Physicochemical and Engineering Aspects 2020; 598: 124819.
[34] Sheng JJ. Critical review of low-salinity waterflooding. Journal of Petroleum Science and Engineering 2014; 120: 216–24.
[35] Yousef AA, Al-Saleh S, Al-Kaabi A, Al-Jawfi M. Laboratory Investigation of the Impact of Injection-Water Salinity and Ionic Content on Oil Recovery From Carbonate Reservoirs. SPE Reservoir Evaluation & Engineering 2011; 14: 578–93.
[36] Sun H. COMPASS: An ab Initio Force-Field Optimized for Condensed-Phase ApplicationsOverview with Details on Alkane and Benzene Compounds. J Phys Chem B 1998; 102: 7338–64..
[37] Chang X, Xue Q, Li X, Zhang J, Zhu L, He D, et al. Inherent wettability of different rock surfaces at nanoscale: a theoretical study. Applied Surface Science 2018; 434: 73–81.
[38] Li X, Wang P, Wang S, Feng Q, Xue Q. Dynamics and miscible behaviors of hydrocarbon gas and crude oil in nanoslits: Effects of light gas type and crude oil components. Chemical Engineering Journal 2021; 405: 127012.
[39] Li S, Liu Y, Xue L, Zhu D. Theoretical insight into the effect of polar organic molecules on heptane-water interfacial properties using molecular dynamic simulation. Journal of Petroleum Science and Engineering 2022; 212: 110259.
[40] Sedghi M, Piri M, Goual L. Atomistic Molecular Dynamics Simulations of Crude Oil/Brine Displacement in Calcite Mesopores. Langmuir 2016; 32: 3375–84.
[41] Zhang W, Feng Q, Wang S, Xing X. Oil diffusion in shale nanopores: Insight of molecular dynamics simulation. Journal of Molecular Liquids 2019; 290: 111183.
[42] Li X, Wang P, Yan Z, Yu S, Wei K, Zhu X, et al. The miscible behaviors of C_3H_8/C_8H_{18}($C_7H_{17}N$) system in nanoslits: Effects of pore size and rock surface wettability. Chemical Engineering Journal 2022; 431: 133988.
[43] Xiong H, Devegowda D, Huang L. Water Bridges in Clay Nanopores: Mechanisms of Formation and Impact on Hydrocarbon Transport. Langmuir 2020; 36: 723–33.